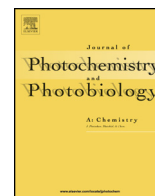




ELSEVIER

Contents lists available at ScienceDirect

Journal of Photochemistry and Photobiology A:  
Chemistryjournal homepage: [www.elsevier.com/locate/jphotochem](http://www.elsevier.com/locate/jphotochem)

Invited feature article

Photoenolization *via* excited state proton transfer and ion sensing studies of hydroxy imidazole derivativesMohammad Shahid<sup>a,b,\*</sup>, Arvind Misra<sup>b,\*\*</sup><sup>a</sup> Department of Chemistry, Indian Institute of Technology Delhi, HauzKhas, New Delhi, India, India<sup>b</sup> Department of Chemistry, Institute of Science, Banaras Hindu University, Varanasi 221005, U.P., India, India

## ARTICLE INFO

## Article history:

Received 29 October 2016

Received in revised form 2 December 2016

Accepted 3 December 2016

Available online 6 December 2016

## Keywords:

ESIPT

Solvatochromism

Photo-enolization

Ionic recognition

Acetate ion

## ABSTRACT

A light stimulated photo-enolization in hydroxy imidazole systems (*o*-hydroxynaphthyl phenanthroimidazole, 3 and *o*-hydroxyphenyl phenanthroimidazole, 4) by excited state proton transfer induces “turn Off” fluorescence and ratiometric changes in the absorption spectrum. Benzyl phenanthroimidazole (5) does not exhibit the photo-enolization due to absence of *o*-hydroxyl group. Solvatochromism, time resolved photoluminescence measurement and ionic interactions studies of 3–5 are examined in semi-aqueous medium through UV–vis and fluorescence spectroscopy. Fluorescent probe 3 exhibits fluorescence “turn Off” and “turn On” responses with acetate ions in semi-aqueous medium by tuning the excitation wavelength.

© 2016 Elsevier B.V. All rights reserved.

## 1. Introduction

The excited state intramolecular proton transfer (ESIPT) and photoinduced proton transfer processes have attracted great attention due to its wide applications in the design and development of luminescent materials, photopatterning, chemosensors, proton transfer laser, photostabilizers, molecular logic gates, molecular probes, metal ion sensors, radiation hard-scintillator counters, organic light emitting devices (OLEDs) and optical devices *etc* [1,2]. The ESIPT chromophores ideally exhibits remarkable Stokes Shift in comparison to the normal fluorophores such as fluorescein, rhodamine or boron-dipyrromethene (BODIPY) [3].

In the ESIPT molecule, large Stokes' shift occurs due to the typical four-level photophysical scheme consisting of the ground (*GS*) and excited (*ES*) states of two different tautomers. In the *GS*, the typical ESIPT molecules prefer to adopt enol form due to thermodynamic stabilization by the intramolecular hydrogen-bonding. However, upon photo-excitation excited *keto* tautomer generate due to the fast proton transfer reaction (picoseconds

level) from the excited *enol* form. After decaying to the ground state, the excited *keto* form reverts to the original *enol* form *via* reverse proton transfer. Thus, in an ESIPT cycle the absorbing and emitting molecular species leads to the total exclusion of self-absorption and the large Stokes' shifted *keto* emission [4]. Therefore, fluorescence due to ESIPT process is an effective tool in fluorescence based applications and large Stokes' shift is a desired feature for fluorophores to minimize the self-absorption or the inner filter effect [5]. Moreover, the ESIPT process is much faster than the fluorescence process (radiative decay), and the observed fluorescence by the ESIPT chromophores is primarily due to the *keto* tautomer with some exceptions [6]. Thus, the ESIPT process is accompanied by a remarkable geometry relaxation between *keto* and *enol* tautomers. The ESIPT molecules have some limitations such as, short excitation wavelength despite of their long Stokes' shift, sensitive to environment, and in protic medium the emission of ESIPT sensitive chromophores get perturbed [5,7]. For instance, in protic solvents, the ESIPT emission due to *keto* form (ca. 500 nm) usually diminished, and the emission due to the *enol* form dominates at low wavelengths [5,7].

The fundamental photoinduced electron and proton transfer processes are generally prevalent in *keto-enol* and *azo-phenol* systems due to possibility of intramolecular hydrogen bonding between hydrogen-bond donors (acidic proton) such as —OH, —NH and hydrogen-bond acceptors (basic moiety) such as —N: and —C=O functions present in an aligned geometry [8]. Excitation to first excited state leads to a change in charge density, increase in

\* Corresponding author at: Department of Chemistry, Indian Institute of Technology Delhi, HauzKhas, New Delhi, India.

\*\* Corresponding author. Tel.: +91 542 2307321x104/6702503; fax: +91 542 2368127/2368175.

E-mail addresses: [shahidchem@gmail.com](mailto:shahidchem@gmail.com) (M. Shahid), [arvindmisra2003@yahoo.com](mailto:arvindmisra2003@yahoo.com), [amisra@bhu.ac.in](mailto:amisra@bhu.ac.in) (A. Misra).

acidity and basicity of two complementary centers due to which ultrafast migration of a proton through a hydrogen bond coordinate is possible to develop photo-tautomers each having different and specific electronic distribution and optical properties accordingly.

Furthermore, the most of anion recognition studies involve hydrogen bond interaction between the anion and receptor molecule. Also, the sensing ability of a specific receptor system depends on the affinity of interaction with a guest species, geometry of the molecule/complex, physico-organic nature of analytes and microenvironment. Therefore, harnessing the ESIPT process for development of new anion binding signaling systems seems promising [9]. In view of the fact that anions like, carboxylate, fluoride and phosphate play significant roles in chemical, environmental and biochemical processes [10,11]. Particularly, carboxylates are critical components for numerous metabolic processes [11c] and exhibit specific biochemical behavior in enzymes and antibodies. Therefore, the design and synthesis of effective small organic molecular scaffolds having a suitable receptor site to recognize specific analyte sensitively through good output optical signal are in great demand and interesting in the area of supramolecular chemistry [10].

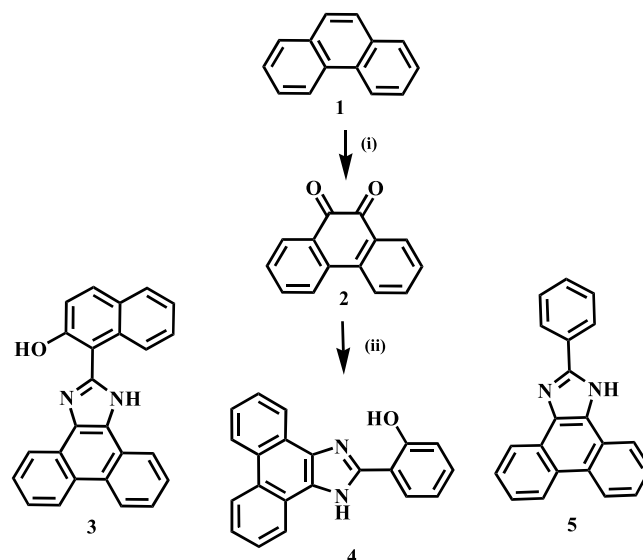
In this communication, to study the ESIPT mechanism we have developed phenanthroimidazole based molecular probes **3** and **4** that are capable to show strong intramolecular H-bonding, solvatochromism and photo-enolization processes. The potential probe **3** is conjugated with naphthalene moiety for extending  $\pi$ -conjugation to gain large Stokes' shift (useful to avoid self-absorption), better electronic transition from *keto* tautomer with enhanced energy gap between ground and excited state, and quantum yield and sensitive to detect specific anion. The chemical design of compounds **3** and **4** are based on hydroxyl imidazole system to promote intramolecular H-bonding between  $-OH$  and  $=N-$  functions through a stable six membered cyclic ring and stability in host-guest interaction. The synthesized model compound **5** due to the absence of  $-OH$  function is unable to exhibit photo-enolization. The probes **3** and **4** are able to recognize acetate ions selectively through a change in color, UV-vis, fluorescence and  $^1H$  NMR spectra. Probe **3** on interaction with  $AcO^-$  induces a fluorescence "turn-Off" and "turn-On" behavior when excited at 365 and 411 nm respectively with a high association constant and favorable response time.

## 2. Results and discussion

### 2.1. Synthesis

The synthesis (Scheme 1) of *o*-hydroxynaphthyl phenanthroimidazole (**3**), *o*-hydroxyphenyl phenanthroimidazole (**4**) and benzyl phenanthroimidazole (**5**) have been carried by reacting 9,10-phenanthroquinone, **2** in ethanol with corresponding aldehyde (2-hydroxy-1-naphthaldehyde, salicylaldehyde and benzaldehyde respectively) in presence of ammonium acetate ( $AcONH_4$ ) and iodine (as catalyst). Compound **2** was obtained in good yield by the oxidation of phenanthrene, **1** with  $Na_2Cr_2O_7$  in acetic acid. All the derivatives were characterized by different spectroscopic data analysis (Fig. S1-12).

The UV-vis absorption spectrum of **3**, **4** and **5** ( $1 \mu M$ ) in aqueous-MeCN (20%, v/v) shows absorption bands at  $\lambda_{max}$  365, 362 and 359 nm ( $\epsilon = 23066, 30370, 13911 M^{-1} cm^{-1}$ ) along with high energy bands at 318, 331 and 311 nm, respectively. The low energy,  $n \rightarrow \pi^*$  electronic transition band appeared at  $\lambda_{max} \sim 365$  nm is ascribed to charge transfer (CT) while the high energy band observed may be attributed to  $\pi \rightarrow \pi^*$  electronic transitions [12]. The emission spectra of **3** and **4** illustrated emission maxima at  $\lambda_{em} \sim 464$  nm with Stokes' shift of  $1.01 \times 10^5$  and  $1.05 \times 10^5 cm^{-1}$



**Scheme 1.** Synthesis of 3–5. (i)  $Na_2Cr_2O_7/AcOH/\Delta$ , (ii)  $AcONH_4/aldehyde/EtOH/\Delta$ .

on excitation at  $\sim 365/362$  nm respectively. While **5** exhibited emission maxima at 421 nm with a lesser Stokes' shift on excitation at 360 nm.

### 2.2. Solvatochromism

#### 2.2.1. Steady-state UV-vis absorption and emission spectra

The solvent dependent analysis was monitored for **3**, **4** and **5** in different non-polar, polar aprotic and polar protic solvents such as hexane, DCM, MeCN, DMSO, MeCN/ $H_2O$  and MeOH which has been summarized in Table 1. The UV-vis absorption spectra of **3** and **4** exhibits hypsochromic shift (blue shift) on increasing solvent polarity i.e. hexane to MeOH (Fig. S13). Absorption maxima of **3** appeared at 373 and 374 nm in hexane and DCM, respectively. In MeCN and DMSO absorption maxima obtained at 370 and 368 nm while in MeCN/ $H_2O$  and MeOH, it was found at 365 and 360 nm. For **4** and **5**, similar trends were observed in absorption spectra and absorption maxima appeared at 337–332 and 314–308 nm from non-polar to polar protic solvents respectively (Fig. S14, 15).

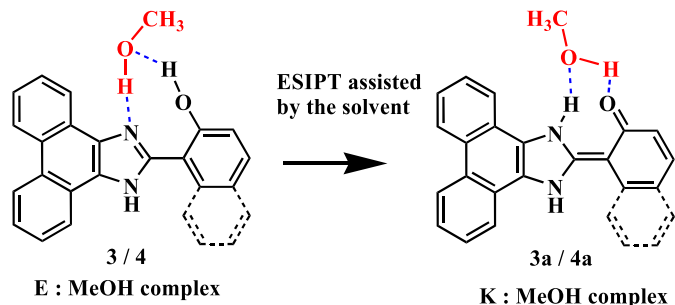
Fluorescent behavior of molecular receptors **3–5** were evaluated in solvents of different polarities (Fig. S16–20). In non-polar/less polar solvents, the emissions maxima of **3** appeared at  $\sim 524$  nm (in DCM) and at  $\sim 495$  nm (in hexane). In MeCN and DMSO, the emission band appeared at 518 and 507 nm respectively whereas, in polar protic solvent (MeOH), it appeared at 482 nm (Fig. S16). Similarly, the emissions spectra of **4** showed dual emission bands at  $\sim 420$  and  $\sim 530$  nm due to intramolecular charge transfer (ICT) and ESIPT processes, respectively. The emission spectra in hexane shows maxima at 515 nm whereas, in DCM, MeCN and DMSO it appeared at 533, 523 and 533 nm, respectively (Fig. S17). Thus in hexane, DCM, MeCN, DMSO and MeOH solutions, the observed blue emission band is possibly for *enol* tautomer while, the longer wavelength emission is attributed to a *keto* tautomer as a result of ESIPT mechanism [1a,8b,c]. The emission band in MeOH blue shifted to appear at 514 nm and is similar to the data obtained from already reported probes demonstrating ESIPT [13c,14]. The observed photophysical changes may be rationalized to the intermolecular hydrogen bonding with methanol molecule leading to the stabilization of solvated isomer making the ESIPT reaction of **3** and **4** slower via a proton-relay (Scheme 2) [8b].

Moreover, the observed colorimetric changes for probe **3** and **4** under UV light is probably due to variable ratio between *keto* and *enol* emissions in different solutions (Fig. S19). Probe **5** shows the

**Table 1**  
Spectroscopic parameters for probes 3–5.

s.n.	Solvents	3					4					5				
		$\lambda_{\max}$ (nm)	$\lambda_{\text{em}}$ (nm)	$\Delta\nu$ (nm)	$\epsilon$	$\Phi$	$\lambda_{\max}$ (nm)	$\lambda_{\text{em}}$ (nm)	$\Delta\nu$ (nm)	$\epsilon$	$\Phi$	$\lambda_{\max}$ (nm)	$\lambda_{\text{em}}$ (nm)	$\Delta\nu$ (nm)	$\epsilon$	$\Phi$
1	Hexane	373	495	130	2.90	0.329	337	515/434	180	1.53	0.662	314, 403	403	83	3.21	0.121
2	DCM	374	524	159	1.53	0.634	336	533/424	198	2.76	0.345	314, 417	417	97	3.10	0.091
3	MeCN	370	518	153	3.36	0.256	332	523/424	188	2.35	0.382	312, 406	406	86	2.72	0.109
4	DMSO	368/394	507	142	0.97	0.832	335	533/428	198	2.34	0.493	315, 426	426	106	2.94	0.101
5	MeCN/H <sub>2</sub> O	365	498	133	2.30	0.504	331	–	–	3.03	0.295	311, 421	421	101	3.21	0.090
6	MeOH	360	482	117	1.03	0.643	332	514/411	179	1.96	0.469	308, 400	400	80	2.94	0.102

Note:  $\epsilon$  is the molar extinction coefficient (in  $10^5 \text{ cm}^{-1} \text{ M}^{-1}$ );  $\Phi$  is the quantum yield with respect to Quinine sulphate and  $\Delta\nu$  is the Stokes Shift (nm).



**Scheme 2.** Possible molecular structure of 3/4 and 3: MeOH/4: MeOH complex which restrict the ES IPT process.

emission maxima between  $\sim 403$  and  $426$  nm for hexane to DMSO and in protic solvent at  $400$  nm. It was unable to show the high Stokes' shift emission band (ES IPT band,  $>480$  nm) (Fig. S20). The change in solvent polarity shifted the spectra toward shorter wavelength region probably due to H-bonding with the lone pair electron of the probes and polar solvent, in the ground state. While, in the excited state, hydrogen bonding involves only one electron of the lone pair (the other have been promoted to an upper energy state). Thus, due to relatively more stabilized ground state than the excited state, absorption shifted to the short wavelength region.

### 2.3. Spectral behavior of 3 at different pHs

Since ES IPT molecules have amphoteric properties due to the presence of both Lewis acidic  $\text{—NH—/—OH}$  and basic  $\text{=N—}$  sites in the imidazole ring. Probe 3 has both the proton donor and acceptor group that can be protonated or deprotonated depending on pH of the solution [1a]. Therefore, we intended to examine the photo-physical behaviour of 3 at different pHs in aqueous acetonitrile. The UV–vis absorption spectrum of 3 ( $1 \mu\text{M}$ ) in aqueous–acetonitrile

(50%, v/v) displayed absorption band at  $365$  nm with a shoulder at high energy band at  $310$  nm. Probe 3 displayed a dual emission band at  $410$  and  $498$  nm with a large Stokes' shift ( $133$  nm) (Fig. 1). On changing the pH of the medium from 7 to 1, the absorption spectra showed a blue shift of  $15$  nm along with a marginal decrease in molar absorption while under alkaline condition (pH 12), the absorption band centred at  $365$  nm diminished with a new red shifted absorption maxima at  $409$  nm. Moreover, the emission spectra of 3 in the acidic medium (pH 1) showed emission band at  $445$  nm with a hypsochromic shift of  $\sim 48$  nm (with a Stokes' shift of  $80$  nm). However, in basic medium (pH 12), emission band appeared at  $508$  nm with a red shift of  $10$  nm (with a Stokes' shift of  $143$  nm). Probe 3 in basic medium (pH 12) forms an anionic species resulting in a red-shifted absorption and emission band due to increase in conjugation or delocalization. In acidic medium, 3 was protonated (hydroxyl or amino group) which reduces the conjugation/delocalization resulting blue shift in the spectrum (Scheme 3). Thus, in the acidic and basic pH conditions ES IPT reaction was inhibited [13]. The pH dependent studies of probe 4 was reported by Plass et al., where deprotonation of  $\text{—NH/—OH}$  unit possibly occurred in basic condition [14a]. In the alkaline medium where deprotonation of the molecule took place, *o*-hydroxyl imidazole gave lower  $\text{pK}_a$  values ( $\text{pK}_a \sim 11.00$ ) than the non-hydroxyl one, 5 ( $\text{pK}_a \sim 13.50$ ). Therefore, the observed anionic states in alkaline media for the compounds bearing hydroxyl groups (3 and 4) are due to the phenolic proton removal (Scheme 3) while the anions of non-hydroxyl analogues (5) resulted from imidazole  $\text{—NH}$  deprotonation [14a].

Probes 3 and 4 having intramolecular hydrogen bonds between  $\text{—OH}$  and  $\text{—C=N—}$  group, so there could be existence of ES IPT phenomenon in the systems. The most stable form of ES IPT molecules in the ground state is in equilibrium between different conformers arising from tautomerism and rotamerism as reported by Nayak [14b]. The normal planar form of the probes features an intramolecular hydrogen bond between protic acidic group *i.e.*

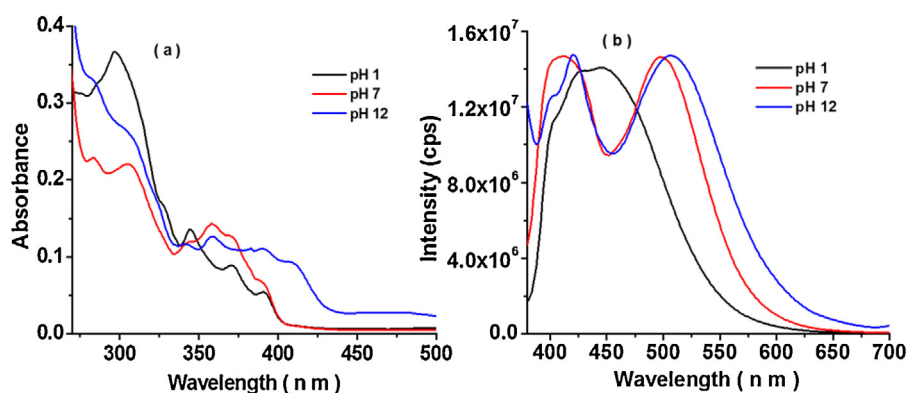


**Fig. 1.** Spectral behavior of 3 at different pHs in aqueous-acetonitrile (50%, v/v).

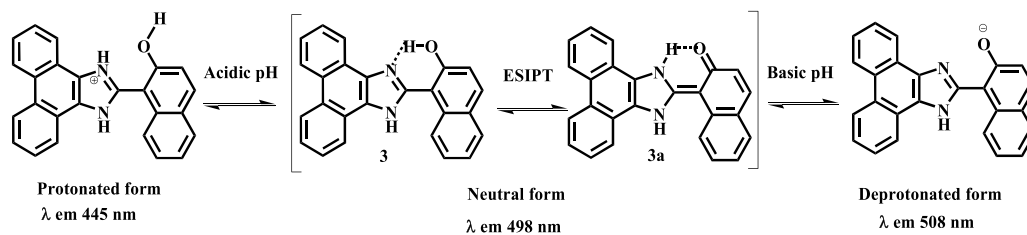
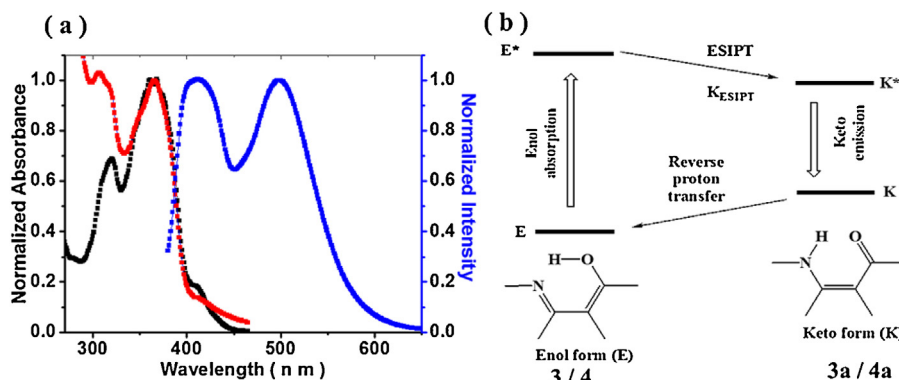
Scheme 3. Prototropic equilibria of **3**.

Fig. 2. (a) Normalized absorption (red), emission ( $\lambda_{\text{ex}}=365$ ; blue) and excitation ( $\lambda_{\text{em}}=498$  nm; black) spectra of **3** in aqueous acetonitrile. (b) Schematic representation shows 4 step ESIPT mechanism. (For interpretation of the references to colour in this figure legend, the reader is referred to the web version of this article.)

hydroxyl and the basic nitrogen atom of the imidazole ring. The normal planer conformer (**3** and **4**) can undergo a rapid proton transfer to form its tautomer (**3a** and **4a**). Upon excitation of the normal form to its first excited singlet state, undergoes an ultrafast excited state intramolecular proton transfer to yield planer tautomer (**3a** and **4a**) accompanied with fluorescence spectra showing large Stokes shift (Fig. 2b). The derivative **5** did not possessed *o*-hydroxy group and therefore could not able to exhibit the ESIPT phenomenon.

Fig. 2a shows the normalized absorption, excitation and emission spectra of **3**. The normalized electronic transition spectra of **3** showed a low energy absorption band at 365 nm with a high energy band at 310 nm due to the presence of phenolic and quinonoid forms in the medium respectively. Similarly, the normalized emission spectrum of **3** due to  $S_0 \rightarrow S_1$  ( $\pi \rightarrow \pi^*$ ) transition showed emission at 498 nm with high Stokes shift (133 nm). However, when the excitation spectra were acquired

at  $\sim 495$  nm excitation the observed emission band was almost structurally identical to the absorption spectra of **3**. It clearly suggested that the emission has originated from the same ground state species [13]. These observation clearly indicated that due to the presence of hydroxyl imidazole moiety, the emission of **3** proceed *via* excited state intramolecular proton transfer (ESIPT) in the  $\pi \rightarrow \pi^*$  state during the period of low-frequency vibrational motions associated with the hydrogen bond [13b]. Thus, it is worth to mention that the enhanced emission observed is due to the dominance of quinonoid form which remain in the equilibrium with H-bond stabilized phenolic form, as well as due to deprotonation and protonation of **3** in the alkaline and acidic conditions, respectively.

### 2.3.1. Time-Resolved spectroscopic study

Fluorescence excited state lifetimes are very sensitive to the structure and dynamics of a fluorophore. Fluorescence decay profiles of **3** and **4** were obtained in aqueous-acetonitrile solution (Fig. 3). Double exponentially decaying constants with short ( $\tau_1$ ) and long ( $\tau_2$ ) decay components were observed and summarized in Table (S1, S2). The lifetime decay profile of probe **3** and **4**, showed two decay constants however, the dominant component was due to the fast decay constant  $\tau_1$ . In case of **3**, the numerical values of  $\tau_1$  and  $\tau_2$  were 0.25 and 1.96 ns respectively. The relative contributions from these components were 6.36% and 93.64% for  $\tau_1$  and  $\tau_2$ , respectively and the average lifetime ( $\tau_0$ ) was calculated as 1.85 ns. While, in case of **4**, the numerical values of  $\tau_1$  and  $\tau_2$  were 0.60 ns and 2.44 ns respectively. The relative contributions from these components were 4.78% and 95.22% for  $\tau_1$  and  $\tau_2$  respectively and the average lifetime ( $\tau_0$ ) was calculated as 2.34 ns. Moderate lifetime value as well as high quantum yield of **3** and **4** suggested that the rate of non-radiative decay ( $\kappa_{\text{nr}}$ ) is not large in **3** and **4**. This can also be explained by the formation of intramolecular hydrogen bond between phenolic  $-OH$  and imidazole *N*, which seems to produce certain amount of rigidity in the system and hence suppresses the non-radiative decay pathways [15].

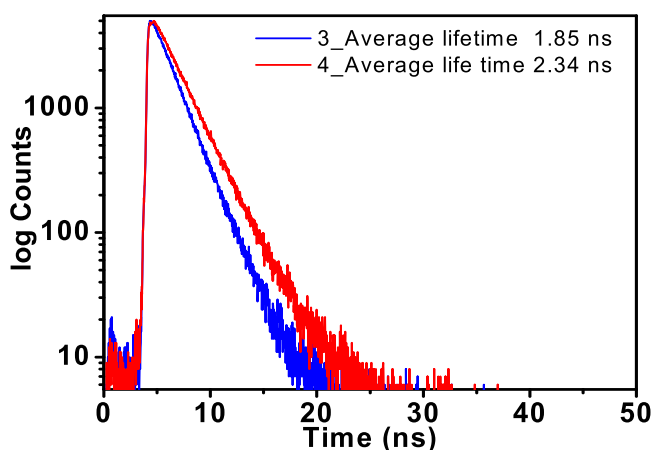


Fig. 3. Fluorescence decay profile of **3** and **4** ( $10 \mu\text{M}$ ) in aqueous acetonitrile solution, measurement conditions:  $\lambda_{\text{ex}}=377$  nm and  $\lambda_{\text{em}}=470$  nm.

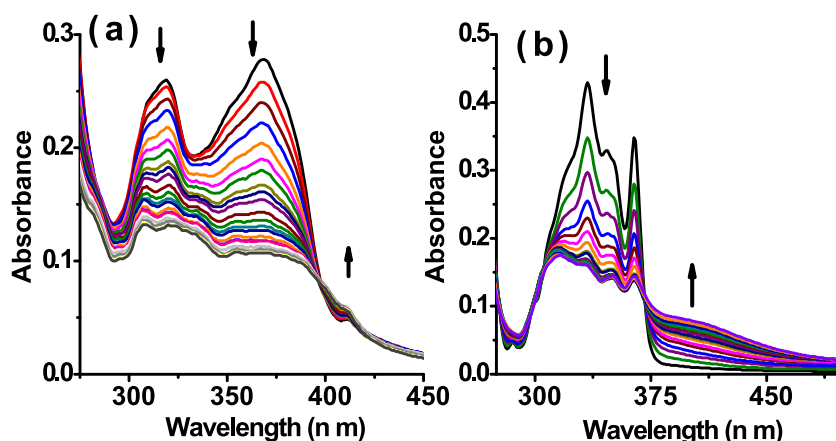


Fig. 4. Change in absorption spectra of (a) **3** and (b) **4** ( $1 \mu\text{M}$ ) upon photo-irradiation of  $\lambda$  365 nm in tetrahydrofuran.

#### 2.4. Photo-enolization

Hydroxy imidazole systems are known to illustrate the *keto-enol* tautomerism. In order to understand the potentiality for such kind of phenomena in the present studies, solutions of **3** and **4** were prepared ( $1 \times 10^{-6}$  M) in an aprotic solvent such as tetrahydrofuran (THF) and were taken in a sealed 1 cm path length quartz cuvette [8d]. Each vial has given UV exposure of 365 nm (UV lamp, GeNei) for a definite time intervals at room temperature and the absorption and emission spectra were acquired. Upon photo-irradiation at 365 nm (Fig. 4), the absorption spectra of **3** was steadily modulated and molar extinction coefficient corresponding to both high ( $\pi \rightarrow \pi^*$ ) electronic transition bands centered at 317 and 368 nm were decreased. After 650 s of photo-irradiation, the low energy band was completely disappeared and concomitantly a shoulder was appeared at 425 nm with an isosbestic point at 399 nm. The color of solution was changed from yellow to a light yellow. Similarly, **4** upon photo-irradiation, the absorption bands centered at 335 and 365 nm were reduced ratio metrically and a new broad band at 420 nm generated concomitantly with an isosbestic point at 374 nm. The presence of isosbestic points is in agreement with the structural transformation of the **3** and **4** between the *Keto* and *Enol* forms [8d].

The photo-irradiation experiment was also examined by emission spectroscopy. The probes **3** and **4** were subjected to photo-irradiation for stipulated time intervals as mentioned above at  $\sim 317$  nm in THF. The relative fluorescence intensity of **3** at 468 nm decreased gradually and disappeared completely with the generation of a new band at 376 nm. The isoemissive point

appeared at 395 nm illustrated the conversion of one form of molecule to another form. Similarly, when **4** was subjected to photo-irradiation for approximately 500 s, the strong emission band centered at 465 nm quenched almost completely without formation of a new band (Fig. 5) while the **5** could not show any change on photo-irradiation under similar experimental condition (Fig. S21).

Moreover, the photochromic behavior of **3** and **4** were further examined by  $^1\text{H}$  NMR spectra before and after the photo-irradiation at 365 nm UV exposure. Before irradiation, the  $^1\text{H}$  NMR spectra of **3** and **4** were sharp and well resolved whereas, after irradiation  $^1\text{H}$  NMR spectra displayed additional resonance signals indicating the presence of a mixture of isomers, possibly the *keto* and its newly formed species with broadened resonance signals (Fig. S22, 23, 23a). Further, HRMS spectra were also acquired before and after photo-irradiation (Fig. S24–27). The appearance of same molecular ion peak even after photo-irradiation, suggested no degeneration of probe, and at same time suggested about the conformational change in the medium. The observed photophysical changes upon photo-irradiation and generation of new band in the absorption, emission and  $^1\text{H}$  NMR spectra of **3** and **4** are attributed due to (i) *keto-enol* tautomerization by proton transfer from the  $-\text{OH}$  of phenol to  $-\text{C}=\text{N}-$  group of imidazole to generate *enol* and (ii) *syn-anti* isomerization of the  $-\text{OH}$  function with respect to  $-\text{C}=\text{N}-$  [16].

#### 2.5. Quantum chemical calculations

Experimental observations and their possible structure were analyzed by quantum chemical calculations. The geometry

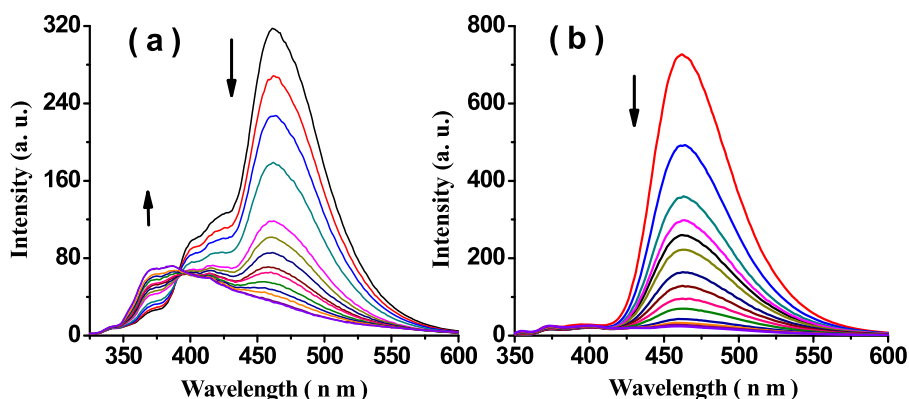


Fig. 5. Change in emission spectra of (a) **3** and (b) **4** ( $1 \mu\text{M}$ ) upon photo-irradiation of  $\lambda$  365 nm in THF.

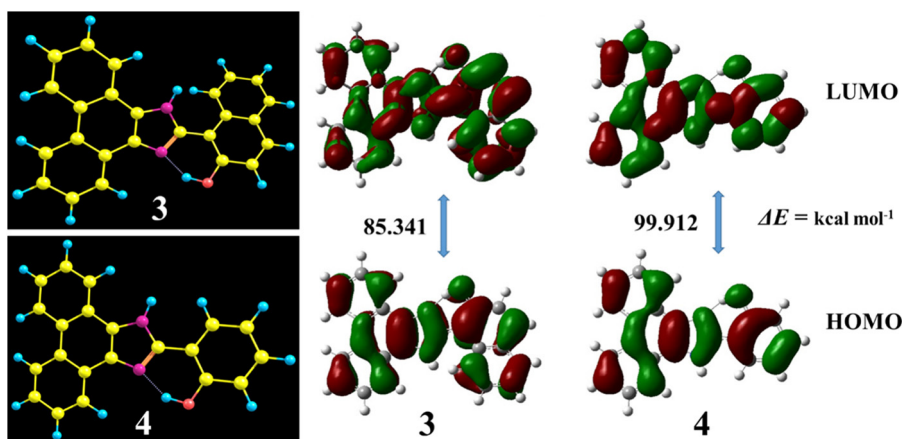


Fig. 6. DFT Optimized minimum energy structure of 3 and 4 as well as their HOMO-LUMO diagram.

optimization were performed for probe **3** and **4** using density functional theory (DFT) method as implemented in Gaussian 03 suits of program [17]. A 6–31G(d,p) basis set was used for all the atoms. DFT calculation was carried to calculate the energy the tautomeric form of both probes **3** and **4** (Fig. 6). The short distance of 1.692 and 1.724 Å between imidazole (=N–) and hydrogen (–OH) suggested about the possibility of strong intramolecular –O–H–N– hydrogen bonding, which favors the mobility of the proton from –OH to Lewis base =N– sites present in the imidazole center. The bond distance for **3** and **4** between –O and aromatic carbon is 1.338 and 1.334 Å, and between –O and –H is 0.998 and 0.994 Å respectively. The calculation results revealed that both the highest occupied molecular orbital (HOMO) of **3** and **4** were mainly distributed over the whole conjugated backbone whereas, the lowest unoccupied molecular orbital (LUMO) primarily resided on the imidazole and hydroxyl part. In case of **4**, the HOMO and LUMO mainly distributed over whole conjugated system. The HOMO and LUMO energies gap were calculated for **3** and **4** and was found to be 85.341 and 99.912 kcal mol<sup>–1</sup> respectively (Fig. 6).

### 2.6. Ion recognition properties of 3–5 with anions

The anion sensing ability of **3**, **4** and **5** were examined through UV–vis absorption spectroscopy after the addition of different anions such as, Br<sup>–</sup>, Cl<sup>–</sup>, F<sup>–</sup>, I<sup>–</sup>, SCN<sup>–</sup>, H<sub>2</sub>PO<sub>4</sub><sup>–</sup>, HSO<sub>4</sub><sup>–</sup>, N<sub>3</sub><sup>–</sup> and AcO<sup>–</sup> (as their tetrabutyl ammonium salts) to a solution of **3–5** in aqueous-acetonitrile (20%, v/v). Upon addition of AcO<sup>–</sup> (5 equiv) to

a solution of **3–5**, a prominent change in the absorption spectra of **3** and **4** were observed in which the transition band at ~365 nm disappeared and concomitantly, a new band appeared at 411 and 390 nm respectively (Fig. 7). The observed red-shift of 46 and 32 nm respectively is attributed to the increase in intramolecular charge transfer from receptor site (–OH/–NH) to phenanthrene ring. Also, the probe **3** showed considerable spectral change with fluoride ion in anhydrous acetonitrile solution but could not in H<sub>2</sub>O–ACN (Fig. S28). Addition of other tested anions to the solution of **3** and **4**, showed no considerable change in the absorption spectra due to comparable high solvation energies of anions<sup>18a</sup> thereby suggested about the specificity of **3** and **4** for selective interaction with AcO<sup>–</sup> in semi-aqueous medium. The model compound **5** could not show any considerable change with tested anions in aqueous–MeCN solution (Fig. S29a). Similarly, the emission band observed at 464 nm for **3** (at λ<sub>ex</sub> 365 nm), illustrated significant fluorescence quenching (68.4%) in presence of AcO<sup>–</sup> (5 equiv). However **4** and **5** exhibited insignificant change in the emission spectra (Fig. 8, S29b). The observed dual mode of emission spectra in absence and presence of AcO<sup>–</sup> clearly suggested different mode of interaction of **3** in the medium that can be accounted by assuming inhibition of ESIPT process due to formation of anionic species or H-bonded complex with acetate ions.

In order to understand the binding affinity of **3** with AcO<sup>–</sup>, absorption and emission titration experiments were performed. From Fig. 9, it can be seen that as concentration of AcO<sup>–</sup> (0–5 equiv) is increased to a solution of **3**, the absorption band at 364 nm

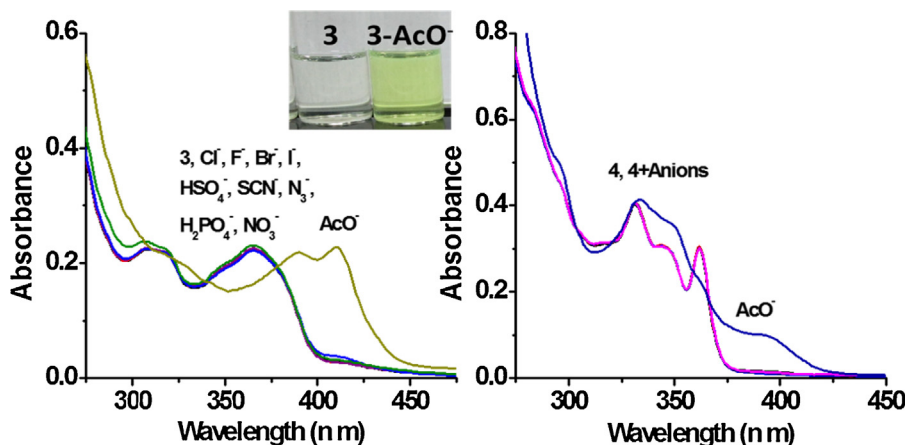


Fig. 7. Change in Absorption spectra of 3 and 4 (1 μM) upon addition of different anions (5 equiv) in aqueous-acetonitrile.

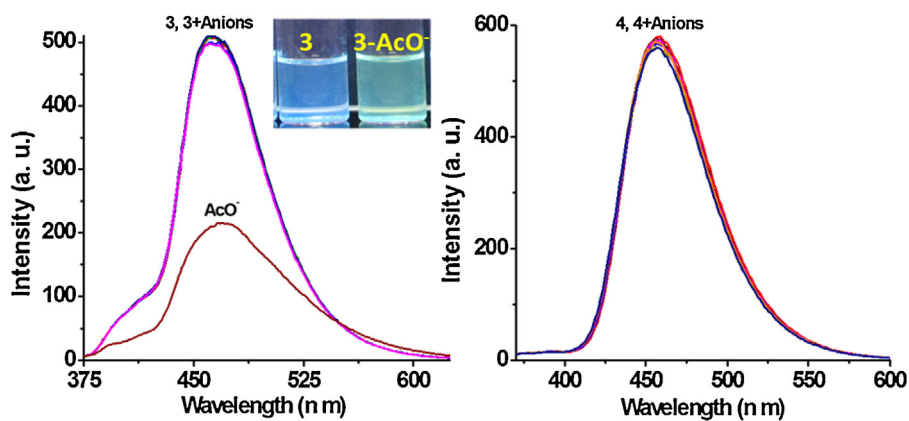


Fig. 8. Change in emission spectra of **3** and **4** ( $1 \mu\text{M}$ ) upon addition of different anions (5 equiv) in aqueous-acetonitrile.

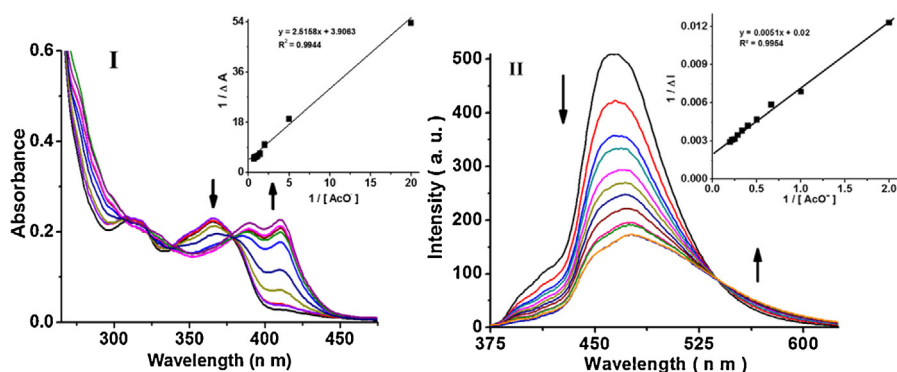


Fig. 9. Absorption (I) and emission (II) titration spectra of **3** with  $\text{AcO}^-$  ions (0–5 equiv) in aqueous-acetonitrile.

reduced gradually with concomitant formation of a new band at 411 nm while in emission spectra, the band centered at 464 nm, quenched gradually with enhancement of a shoulder at 550 nm. The formation of isosbestic points at 378, 339 nm and isoemissive point at 537 nm suggested the generation of a new species in the solution. The observed red shifted low energy absorption band was probably due to interaction of acetate anion with receptor site (N–H and O–H) of **3** that increase the intramolecular charge transfer (CT) and inhibit ESPT processes. The naked eye visible color of the solution changed from colorless to yellow. The Job's plot analysis revealed a 1:1 stoichiometry between **3** and  $\text{AcO}^-$  with association constant, calculated by non-linear fitting of absorption and emission titration data, as  $K_{\text{assoc.}} = 1.03 \times 10^6$  and  $3.92 \times 10^6/\text{M}$  respectively (inset of Fig. 9). Additionally, the limit of

detection (LOD) of **3** for  $\text{AcO}^-$  was estimated in aqueous-MeCN (Fig. S30) by our previously reported method [18]. The estimated  $0.025 \mu\text{M}$  (25 nM) LOD was found comparable to other reported methods and well in limit, as suggested by EPA.

Further, to explore the ionic recognition property of **3** with acetate ions, fluorescence titration experiments were examined on excitation at 380 (isosbestic point) and 411 nm (newly formed band in absorption spectra). At 380 nm excitation, the emission band observed at 464 nm exhibited fluorescence quenching while intensity at  $\sim 560$  nm enhanced ratiometrically with the formation of isoemissive point at 514 nm. While on excitation at 411 nm, **3** showed weak emission spectrum however on increasing concentration of  $\text{AcO}^-$ , the fluorescence enhancement observed at 478 nm due to increase in charge transfer (CT) (Fig. 10). Further, titration of

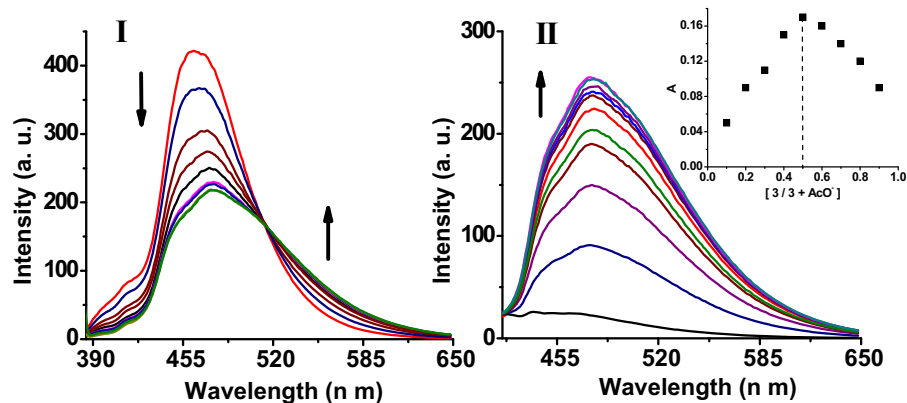


Fig. 10. Emission titration spectra of **3** with  $\text{AcO}^-$  ions (0–5 equiv) in aqueous-acetonitrile at excitation (I) 380 and (II) 411 nm. Inset shows the Job's plot.

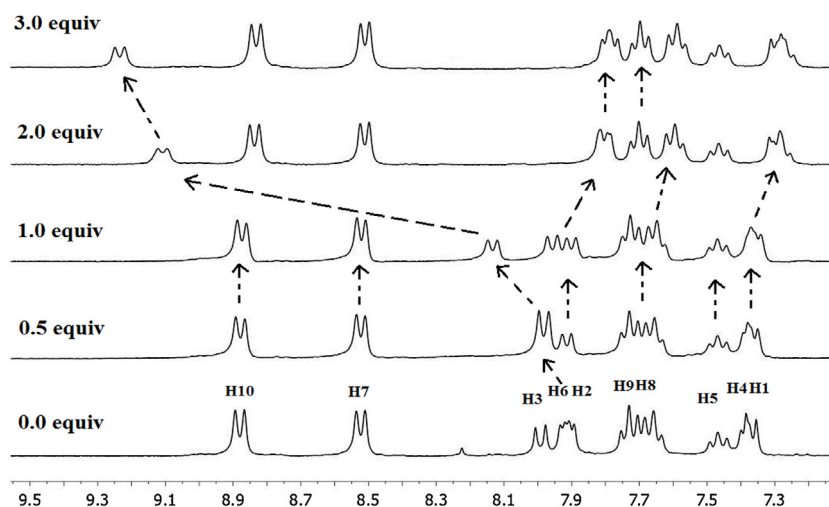


Fig. 11.  $^1\text{H}$  NMR titration spectra of **3** with acetate ions (0.0, 0.5, 1.0, 2.0 and 3.0 equiv) in  $\text{DMSO-}d_6$ .

**3** with acetate ions was examined through excitation spectra at emission band of 465 nm. The excitation band was found at 365 nm (similar to their UV spectrum) on addition of different concentrations of acetate ions (0–5 equiv), in which the band at 365 nm decreased and a new band appeared at 410 nm (Fig. S31).

### 2.7. Sensing mechanism of **3** with $\text{AcO}^-$ anion

The probable binding mechanism of **3** with  $\text{AcO}^-$  was examined by  $^1\text{H}$  NMR titration experiment (Fig. 11, S32). The  $^1\text{H}$  NMR spectrum of **3** ( $2.3 \times 10^{-2}\text{M}$ ) in  $\text{DMSO-}d_6$  showed resonance for phenanthrene protons H10, H7 at  $\delta$  8.89, 8.53 (d) ppm and for H9, H8 protons  $\delta$  7.75 (t) ppm which was primarily overlapped. The naphthalene ring protons resonance appeared at  $\delta$  8.0 ppm (H3, doublet) while H6 and H2 protons merged to appear at  $\delta$  7.93 ppm. The resonance appeared at  $\delta$  7.49 (t) is due to H5 proton while a triplet (overlapped) appeared at  $\delta$  7.39 ppm is attributed H4, H1 protons respectively. On addition of  $\text{AcO}^-$  (0.5 and 1.0 equiv) led to a downfield shift for H6 proton. On increasing the concentration of  $\text{AcO}^-$  (2.0 equiv) the H9, H8 proton resonances separated and H8, H1 protons shifted up field ( $\Delta\delta = 0.09$ , 0.08 ppm respectively). However, the H6 proton further down field shifted to appear at 9.12 ppm ( $\Delta\delta = 1.19$  ppm). Further, increase in acetate ions (3.0 equiv) led to an upfield shift corresponding to H1, H2, H3, H4 protons while H6 resonance shifted downfield. Thus, the respective upfield and downfield shifts in the resonances of probe clearly supported about the increase in charge density of the probe probably due to deprotonation of NH fragment in the presence of  $\text{AcO}^-$  ions which is also evidence from observed bathochromic shift in the UV–vis absorption titration spectra with acetate ions (Fig. 12).

### 3. Conclusions

The potential probes **3** and **4** have been synthesized and studied to understand photo-enolization process through the ESIPT mechanism. Probes have shown light triggered enolization of a hydroxy imidazole derivative with fluorescence “turn Off” response and chromogenic ratiometric changes. The solvatochromic studies revealed that ESIPT process is checked in protic solvents as well as in acid-alkaline medium. Fluorescent probes **3** and **4** upon interaction with different class of anions showed high affinity for acetate anion in partial aqueous medium in which, intramolecular H-bonding get interrupted and new H-bonding interaction followed by deprotonation occurred with acetate ion, which ultimately restricted ESIPT pathway. The model compound **5** could not show photo-enolization process and supported our hypothesis.

### 4. Experimental

#### 4.1. Synthesis of 1,10-phenanthroquinone 2

To a heated solution of concentrated  $\text{H}_2\text{SO}_4$  (10 ml),  $\text{H}_2\text{O}$  (30 ml) and phenanthrene (2 gm) at 90–95 °C,  $\text{K}_2\text{Cr}_2\text{O}_7$  (12 gm) was added portion wise during 1 h and reaction mixture was heated for 30 min. After completion of the reaction (monitored through TLC), cold water was added to the reaction mixture and filtered the precipitate followed by washing with water. The precipitate suspended in ethanol (60 ml) and saturated solution of sodium metabisulfide (30 ml) with frequent stirring for 15 min. Cold water (150 ml) was added to the mixture to dissolve the addition product and filtered. In the filtrate part,  $\text{Na}_2\text{CO}_3$  solution (20%, 50 ml) was added to decompose adduct and allowed to precipitate. The

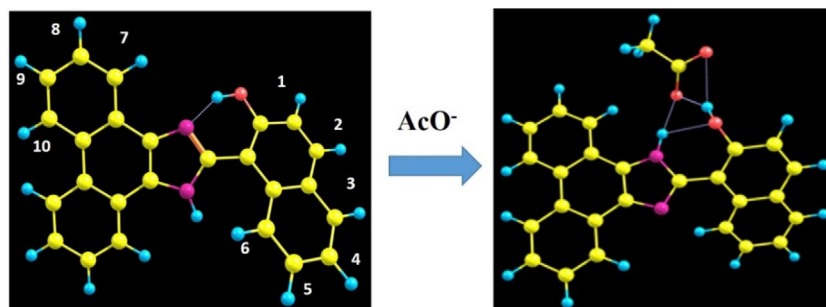


Fig. 12. Probable complexation mechanism of **3** with  $\text{AcO}^-$  ion.

precipitate was filtered followed by washing with water and air dried to obtain orange colored solid. [19]

$R_f = 0.46$  (Ethylacetate:Hexane; 2:8, v/v);  $^1\text{H NMR}$  ( $\text{CDCl}_3$ )  $\delta$  (ppm): 8.23 (d, 2H,  $J = 8.7$  Hz), 7.98 (d, 2H,  $J = 9.0$  Hz), 7.77 (t, 2H,  $J = 8.4, 8.4$  Hz), 7.52 (t, 2H,  $J = 7.2, 7.8$  Hz); FT-IR (KBr)  $\nu_{\text{max}}$  ( $\text{cm}^{-1}$ ) 3023, 1663, 1503, 1442, 1313, 749.

#### 4.2. Synthesis of phenanthroimidazole derivatives (3 to 5)

To a solution of 1,10-phenanthroquinone (0.21 g, 1 mmol) in ethanol (10 ml), corresponding aldehyde (1 mmol),  $\text{AcONH}_4$  (4 mmol) and iodine (5 mol%) were added. The reaction mixture was refluxed for 8 h, after completion of reaction (monitored on TLC) solvent was evaporated under reduced pressure. The cold water was added to the reaction mixture and filtered. The precipitate was washed with cold water and air dried to obtain light yellow solid.

#### 4.3. *o*-Hydroxynaphthyl phenanthroimidazole (3)

$R_f = 0.66$  (Ethylacetate:Hexane; 2:8, v/v);  $^1\text{H NMR}$  ( $\text{CDCl}_3$ )  $\delta$  (ppm): 8.77 (d, 2H,  $J = 8.4$  Hz), 8.48 (d, 1H,  $J = 7.5$  Hz), 8.43 (d, 2H,  $J = 9.6$  Hz), 7.95 (dd, 2H,  $J = 9.9, 7.5$  Hz), 7.76 (m, 4H), 7.47 (t, 1H,  $J = 7.8, 7.5$  Hz), 7.39 (d, 1H,  $J = 9.0$  Hz); FT-IR (KBr)  $\nu_{\text{max}}$  ( $\text{cm}^{-1}$ ) 3400, 2923, 1663, 1623, 1601, 1503, 1442, 1313, 1260, 838, 749; HR-MS calculated for  $[\text{C}_{25}\text{H}_{16}\text{N}_2\text{O} + \text{H}^+]$ : 361.1344 and was found at  $m/z$ : 361.1335.

#### 4.4. *o*-Hydroxyphenyl phenanthroimidazole (4)

$R_f = 0.5$  (Ethylacetate:Hexane; 2:8, v/v);  $^1\text{H NMR}$  ( $\text{CDCl}_3$ )  $\delta$  (ppm): 8.73 (d, 2H,  $J = 8.1$  Hz), 8.55 (d, 2H,  $J = 7.2$  Hz), 8.14 (d, 1H,  $J = 7.8$  Hz), 7.71 (m, 4H), 7.35 (t, 1H,  $J = 7.5$  Hz), 7.15 (d, 1H,  $J = 7.5, 8.4$  Hz), 7.00 (t, 1H,  $J = 6.9, 7.4$  Hz); FT-IR (KBr)  $\nu_{\text{max}}$  ( $\text{cm}^{-1}$ ) 3400, 2923, 1663, 1623, 1601, 1503, 1442, 1313, 1260, 838, 749; HR-MS calculated for  $[\text{C}_{21}\text{H}_{15}\text{N}_2\text{O} + \text{H}^+]$   $m/z = 311.1178$  and found at  $m/z$  311.1182.

#### 4.5. Benzyl phenanthroimidazole (5)

$R_f = 0.7$  (Ethylacetate:Hexane; 2:8, v/v);  $^1\text{H NMR}$  ( $\text{CDCl}_3$ )  $\delta$  (ppm): 8.72 (d, 2H,  $J = 7.5$  Hz), 8.41 (m, 2H), 8.15 (d, 2H,  $J = 6.6$  Hz), 7.68 (m, 4H), 7.47 (m, 4H); FT-IR (KBr)  $\nu_{\text{max}}$  ( $\text{cm}^{-1}$ ) 3300, 2923, 1653, 1626, 1600, 1533, 1421, 1309, 1254, 838, 763.

### Acknowledgement

The author (MS) is thankful to SERB unit of Department of Science and Technology, New Delhi for financial support vide section no. SB/FT/CS-010/2013. The authors are also thankful to the Council of Scientific and Industrial Research (CSIR) (02/0199/14/EMR-II), and Department of Science and Technology (DST-FIST program) New Delhi for financial support. Thanks to Professor Sameer Sapra and Mohd. Samim Hasan, Department of Chemistry, IIT Delhi for their kind support in securing time-resolved fluorescence measurement and Dr. Peter Kapusta, Institute of Macromolecular Chemistry AS CR, 162 06 Prague, Czech Republic for discussion about life time measurement. The authors are also thankful to Dr. Abhinav Kumar, Department of Chemistry, Lucknow University for healthy discussion on DFT optimized structures.

### Appendix A. Supplementary data

Supplementary data associated with this article can be found, in the online version, at <http://dx.doi.org/10.1016/j.jphotochem.2016.12.003>.

### References

- [1] (a) J.E. Kwon, S.Y. Park, Advanced organic optoelectronic materials: harnessing excited-state intramolecular proton transfer (ESIPT) process, *Adv. Mater.* 23 (2011) 3615–3642; (b) K.-C. Tang, M.-J. Chang, T.-Y. Lin, H.-A. Pan, T.-C. Fang, K.-Y. Chen, W.-Y. Hung, Y.-H. Hsu, P.-T. Chou, Fine tuning the energetics of excited-state intramolecular proton transfer (ESIPT): white light generation in a single ESIPT system, *J. Am. Chem. Soc.* 133 (2011) 17738–17745; (c) K.-Y. Chen, C.-C. Hsieh, Y.-M. Cheng, C.-H. Lai, P.-T. Chou, Extensive spectral tuning of the proton transfer emission from 550 to 675 nm via a rational derivatization of 10-hydroxybenzo[h]quinoline, *Chem. Commun.* (2006) 4395–4397.
- [2] (a) J. Catalan, J.C. del Valle, R.M. Claramunt, D. Sanz, J. Dotor, Photophysics of the 2-(2'-hydroxyphenyl)perimidine: on the fluorescence of the enol form, *J. Lumin.* 68 (1996) 165–170; (b) P.S. Sherin, Y.P. Tsentlovich, O.A. Snytnikova, R.Z. Sagdeev, Photoactivity of kynurenine-derived UV filters, *J. Photochem. Photobiol. B* 93 (2008) 127–132; (c) P.S. Sherin, J. Grilj, Y.P. Tsentlovich, E. Vauthey, Ultrafast excited-state dynamics of kynurenine, a UV filter of the human eye, *J. Phys. Chem. B* 113 (2009) 4953–4962; (d) T. Murata, Y. Morita, Y. Yakiyama, K. Fukui, H. Yamochi, G. Saito, K. Nakasui, Hydrogen-bond interaction in organic conductors: redox activation, molecular recognition, structural regulation, and proton transfer in donor–acceptor charge-transfer complexes of TTF-imidazole, *J. Am. Chem. Soc.* 129 (2007) 10837–10846; (e) W.H. Sun, S. Li, R. Hu, Y. Qian, S. Wang, G. Yang, Understanding solvent effects on luminescent properties of a triple fluorescent ESIPT compound and application for white light emission, *J. Phys. Chem. A* 113 (2009) 5888–5895.
- [3] Y. Xu, Y. Pang,  $\text{Zn}^{2+}$ -triggered excited-state intramolecular proton transfer: a sensitive probe with near-infrared emission from bis(benzoxazole) derivative, *Dalton Trans.* 40 (2011) 1503–1509.
- [4] (a) S. Lochbrunner, A.J. Wurzer, E. Riedle, Ultrafast excited-state proton transfer and subsequent coherent skeletal motion of 2-(2'-hydroxyphenyl) benzothiazole, *J. Chem. Phys.* 112 (2000) 10699–10702; (b) S. Takeuchi, T.J. Tahara, Coherent excited state intramolecular proton transfer probed by time-resolved fluorescence, *J. Phys. Chem. A* 109 (2005) 10199–10207; (c) H. Sinha, S. Dogra, Ground and excited state prototropic reactions in 2-(*o*-hydroxyphenyl) benzimidazole, *Chem. Phys.* 102 (1986) 337–347.
- [5] J. Zhao, S. Ji, Y. Chen, H. Guo, P. Yang, Excited state intramolecular proton transfer (ESIPT): from principal photophysics to the development of new chromophores and applications in fluorescent molecular probes and luminescent materials, *Phys. Chem. Phys.* 14 (2012) 8803–8817.
- [6] T. Iijima, A. Momotake, Y. Shinohara, T. Sato, Y. Nishimura, T. Arai, *J. Phys. Chem. A* 114 (2010) 1603–1609.
- [7] J. Seo, S. Kim, S.Y. Park, *J. Am. Chem. Soc.* 126 (2004) 11154–11155.
- [8] (a) S.G. Schulman, Acid-Base chemistry of excited singlet states, in: E.L. Wehry (Ed.), *Modern Fluorescence Spectroscopy*, 239, Plenum Press, New York, 1976; (b) N. Alarcos, M. Gutierrez, M. Liras, F. Sanchez, A. Douhal, An abnormally slow proton transfer reaction in a simple HBO derivative due to ultrafast intramolecular-charge transfer events, *Phys. Chem. Chem. Phys.*, (2015), pp. 16257–16269; (c) N.K. Joshi, P. Arora, S. Panta, H.C. Joshi, Slow excited state phototautomerization in 3-hydroxyisoquinoline, *Photochem. Photobiol. Sci.*, (2014), pp. 929–938; (d) A. Misra, M. Shahid, Chromo and fluorogenic properties of some azo-phenol derivatives and recognition of  $\text{Hg}^{2+}$  ion in aqueous medium by enhanced fluorescence, *J. Phys. Chem. C*, (2010), pp. 16726–16739.
- [9] Y. Abraham, H. Salman, K. Suwinkab, Y. Eichen, Cyclo[2]benzimidazole: luminescence turn-on sensing of anions, *Chem. Commun.* 47 (2011) 6087–6089.
- [10] (a) A.P. de Silva, H.Q.N. Gunarantane, T. Gunnlaugsson, A.J.M. Huxley, C.P. McCoy, J.T. Rademacher, T.E. Rice, Signaling recognition events with fluorescent sensors and switches, *Chem. Rev.* 97 (1997) 1515–1566; (b) R. Martinez-Manez, F. Sancenon, Fluorogenic and chromogenic chemosensors and reagents for anions, *Chem. Rev.* 103 (2003) 4419–4476; (c) A.P. de Silva, D.B. Fox, A.J.M. Huxley, T.S. Moody, Combining luminescence, coordination and electron transfer for signalling purposes, *Coord. Chem. Rev.* 205 (2000) 41–57; (d) E. Kimura, Model studies for molecular recognition of carbonic anhydrase and carboxypeptidase, *Acc. Chem. Res.* 34 (2001) 171–179; (e) Z. Xu, S.K. Kim, J. Yoon, Revisit to imidazolium receptors for the recognition of anions: highlighted research during 2006–2009, *Chem. Soc. Rev.* 39 (2010) 1457–1466.
- [11] (a) A. Misra, M. Shahid, P. Dwivedi, An efficient thiourea-based colorimetric chemosensor for naked-eye recognition of fluoride and acetate anions: UV–vis and  $^1\text{H NMR}$  studies, *Talanta* 80 (2009) 532–538; (b) M. Shahid, P. Srivastava, A. Misra, An efficient naphthalimide based fluorescent dyad (ANPI) for  $\text{F}^-$  and  $\text{Hg}^{2+}$  mimicking OR, XNOR and INHIBIT logic functions, *New J. Chem.* 35 (2011) 1690–1700; (c) T. Gunnlaugsson, A.P. Davis, J.E. O'Brien, M. Glynn, Fluorescent sensing of pyrophosphate and bis-carboxylates with charge neutral PET chemosensors, *Org. Lett.* 4 (2002) 2449–2452.

- [12] F. Rodríguez-Prieto, J.C. Penedo, M. Mosquera, Solvent control of molecular structure and excited-state proton-transfer processes of 1-methyl-2-(2-hydroxyphenyl)-benzimidazole, *J. Chem. Soc. Faraday Trans.* 94 (1998) 2775–2782.
- [13] (a) S. Park, O.-H. Kwon, S. Kim, S. Park, M.-G. Choi, M. Cha, S.Y. Park, D.-J. Jang, Imidazole-based excited-state intramolecular proton-transfer materials: synthesis and amplified spontaneous emission from a large single crystal, *J. Am. Chem. Soc.* 127 (2005) 10070–10074;  
(b) C.Y. Chen, T.-P. Lin, C.-K. Chen, S.-C. Lin, M.-C. Tseng, Y.-S. Wen, S.-S. Sun, Newchromogenic and fluorescent probes for anion detection: formation of a [2+2]supramolecular complex on addition of fluoride with positive homotropiccooperativity, *J. Org. Chem.* 73 (2008) 900–911;  
(c) R. Ali, S.S. Razi, P. Srivastava, A. Misra, Tetrasubstituted imidazole core containing ESIPT fluorescent chemodosimeter for selective detection of cyanide in different medium, *Sens. Actuators B* 221 (2015) 1236–1247.
- [14] (a) A.O. Eseola, O. Adepitan, H. Gorls, W. Plass, Electronic/substituents influence on imidazole ring donor–acceptor capacities using 1H-imidazo[4,5-f][1,10]phenanthroline frameworks, *New J. Chem.* 36 (2012) 891–902;  
(b) M.K. Nayak, Synthesis, characterization and optical properties of aryl and diaryl substituted phenanthroimidazoles, *J. Photochem. Photobiol. A Chem.* 241 (2012) 26–37.
- [15] S. Sinha, B. Chowdhury, P. Ghosh, A highly sensitive ESIPT-based ratiometric fluorescence sensor for selective detection of Al<sup>3+</sup>, *Inorg. Chem.* 55 (2016) 9212–9220.
- [16] (a) K.C.G. Sreedevi, A.P. Thomas, K.H. Aparna, R. Pradhan, M.L.P. Reddy, U. Lourderaj, A. Srinivasan, Photoionization via excited state double proton transfer induces “turn on” fluorescence in diformyl diaryl dipyrromethane, *Chem. Commun.* 50 (2014) 8667–8669;  
(b) C.A. Rice, I. Dauster, M.A. Suhm, Infrared spectroscopy of pyrrole-2-carboxaldehyde and its dimer: a planar beta-sheet peptide model, *J. Chem. Phys.* 126 (2007) 134313–134320;  
(c) B.M. Giuliano, I. Reva, R. Fausto, Infrared Spectra and Photochemistry of Matrix-Isolated Pyrrole-2-carbaldehyde, *J. Phys. Chem. A* 114 (2010) 2506–2517.
- [17] M.J. Frisch, G.W. Trucks, H.B. Schlegel, GAUSSIAN 03, Revision E.01; Gaussian: Wallingford, CT, 2007.
- [18] (a) M. Shahid, S.S. Razi, P. Srivastava, R. Ali, B. Maiti, A. Misra, A useful scaffold based on acenaphthene exhibiting Cu<sup>2+</sup> induced excimer fluorescence and sensing cyanide via Cu<sup>2+</sup> displacement approach, *Tetrahedron* 68 (2012) 9076–9084;  
(b) A. Misra, P. Srivastava, M. Shahid, Fluorescent probe mimicking multiple logic gates and a molecular keypad lock upon interaction with Hg<sup>2+</sup> and bovine serum albumin, *Analyst* 137 (2012) 3470–3478;  
(c) P. Srivastava, R. Ali, S.S. Razi, M. Shahid, A. Misra, Thiourea based molecular dyad (ANTU): fluorogenic Hg<sup>2+</sup> selective chemodosimeter exhibiting blue–green fluorescence in aqueous-ethanol environment, *Sens. Actuators B* 181 (2013) 584–595;  
(d) H.M. Chawla, M. Shahid, D. StC Black, N. Kumar, A new calix[4]arene based molecular probe for selective and sensitive detection of CN<sup>−</sup> ions in aqueous media, *New J. Chem.* 38 (2014) 2763–2765.
- [19] B.S. Furniss, A.J. Hannaford, P.W.G. Smith, A.R. Tatchell, VOGEL's Text Book of Practical Organic Chemistry, fifth edn, Pearson Education Press, 2006, 2016.